

# WAVELET SIGNAL PROCESSING FOR RESOLUTION ENHANCEMENT IN A RECURRENCE TRACKING MICROSCOPE

Naeem Akhtar,<sup>1</sup> Hayat Ullah,<sup>2</sup> Aiman al Omari,<sup>3</sup> and Farhan Saif<sup>2,3,4\*</sup>

<sup>1</sup>*Hefei National Laboratory for Physical Sciences  
Microscale University of Science and Technology of China  
Hefei, Anhui 230026, China*

<sup>2</sup>*Department of Electronics, Quaid-i-Azam University  
Islamabad 45320, Pakistan*

<sup>3</sup>*Department of Physics, Jerash University  
Jerash, Jordan*

<sup>4</sup>*Department of Physics, Quaid-i-Azam University  
Islamabad 45320, Pakistan*

\*Corresponding author e-mail: farhan.saif@fullbrightmail.org

## Abstract

Based on continuous wavelet transform (CWT), we show that the resolution of a recurrence tracking microscope (RTM) is enhanced to subnanometer scale. Our approach helps us to read information on frequency bands, time of revivals, and corresponding time of fractional revivals more accurately. We demonstrate that wavelet analysis provides a deeper information on the phenomena of quantum recurrences in general. Our analytical results show very good agreement with numerical results based on experimental parameters.

**Keywords:** wavelets, multiscale modeling, recurrence tracking microscope, quantum revivals, resolution enhancement, scanning probe microscopy.

## 1. Introduction

Position sensors with nanometer resolution is a major area of current research and has attracted great attention from the scientific community [1–4]. Historically, the development of the electron microscope and scanning probe microscope (SPM), separately based on imaging and sensing of a given sample surface, respectively, has been rewarded the Nobel Prize in 1986 [5]. Resolution enhancement of optical microscopes beyond the diffraction limit has been acknowledged by the award of the Nobel Prize in 2014 to Eric Betzig, Stefan W. Hell, and William E. Moerner [6–8].

Optical microscopes with enhanced resolution have the problem of sample heating and damage to it due to long exposure times. The scanning tunneling microscope (STM) based on quantum tunneling phenomena probes a surface with high accuracy [9, 10]. It has limitations, however, for work on conducting and nonconducting surfaces. Moreover, the impurity atoms introduce unwanted structures in scanning surfaces via STM. The atomic force microscope (AFM), another important form of SPM, has problems due to the diffraction limit.

The recurrence tracking microscope (RTM), based on the phenomena of quantum recurrences, has advantages over STM and AFM [11]. In RTM, the quantum evolution of a wave packet shows revival behavior and reappears when it displays maximum constructive interference and, therefore, partially or completely regains its initial form during the temporal evolution. The phenomena of quantum revival have been studied over the past decades in undriven [?, ?, ?, 12] and driven systems [16].

To enhance the RTM resolution, we consider the signal processing in the frequency domain of a signal  $g(t)$ . This can be obtained, in view of the Fourier transform (FT) [17], as

$$g(\omega) = \int_{-\infty}^{+\infty} g(t)e^{-2\pi i f t} dt. \quad (1)$$

The FT provides the representative frequency components, which are involved in the power spectrum of a signal. Information on time and frequency is simultaneously required in the analysis of a multiple component signal, which we do using the wavelet transform, in order to obtain the time–frequency representation of a signal simultaneously [18].

The wavelet transform is applied to identify the nanotopography of crystal surfaces [19, 20] and to determine the birefringence dispersion in optical fibers [21]. Furthermore, it has been shown that the use of the wavelet transform can be very effective with atomic force microscope (AFM) data analysis [22]. The wavelet transform is also a very useful technique in filtering low-frequency structures in STM [23] for extracting weak signals from a high-noise background [24], in analyzing quantum wave packet dynamics [25, 26], and in quantum field theory [27–30].

In our work, we use the method of continuous wavelet transform (CWT) for the time–frequency analysis of a material wave packet in RTM. We reconstruct each time harmonic of the material wave packet across its frequency, which on the one hand increases the conceptual understanding of the quantum recurrences and on the other hand increases the resolution of RTM. The CWT  $T_{g(t)}(f, \tau)$  of a signal  $g(t)$  can be defined as

$$T_{g(t)}(f, \tau) = \sqrt{f/f_0} \int_{-\infty}^{+\infty} g(t)h^*(f/f_0)(t - \tau) dt,$$

where  $h(t)$  is known as the mother wavelet [18] and the ratio  $(f_0/f)$  is the scaling parameter.

Let us assume that the wavelet is centered at time zero and oscillates with frequency  $f_0$ . The wavelet basis function  $h(f/f_0)(t - \tau)$  has a variable length and width according to frequency  $f$  at different stages  $\tau$  of the signal. The resulting 2D square magnitude display of the transformed function  $T_{g(t)}(f, \tau)$  is known as a scalogram,

$$h(t) = \pi^{-1/4} e^{2\pi i f_0 t} e^{-t^2/2},$$

where  $f_0$  is the central frequency of the wavelet. To construct the translated and dilated Morlet wavelet, we replace  $t$  by  $(f/f_0)(t - \tau)$  to get

$$T_{g(t)}(f, \tau) = \pi^{-1/4} \sqrt{f_0/f} \int_{-\infty}^{+\infty} g(\tau + \zeta f_0/f) e^{-i f_0 \zeta} e^{-\zeta^2/2} d\zeta,$$

where  $\zeta = (f/f_0)(t - \tau)$  and  $T_{g(t)}(f, \tau)$  is the CWT for a signal  $g(t)$ , in view of the Morlet wavelet.

The layout of this paper is as follows.

In Sec. 2, we briefly explain the RTM and calculate the autocorrelation function associated with matter waves. In Sec. 3, the time–frequency representation of the autocorrelation function is carried out using CWT. We dedicate Sec. 4 to resolution enhancement in the RTM by applying the time–frequency analysis developed.

## 2. Matter Waves in RTM

During the time evolution, a material wave packet manifests decoherence and coherence phenomena as it experiences destructive and constructive interference leading to quantum recurrences. As the wave packet follows the classical trajectory in its early evolution, it reconstructs itself after the classical period  $T_{\text{cl}}$ . Thereafter, the wave packet dynamics displays a gradual increase in destructive interference, which results in a collapse of the wave function. We observe quantum revival phenomenon in the long time domain, which is the manifestation of ultimate constructive interference [12].

In the recurrence tracking microscope, we propagate a material wave packet, which experimentally represents a cold atom moving under the gravitational field. The atom bounces off over an atomic mirror made up of an evanescent wave above a dielectric surface, connected with a cantilever. The other end of the cantilever probes the unknown surface. In order to calculate the temporal evolution of the wave packet, we calculate the autocorrelation function, defined as

$$A(t) = \sum_n |a_n|^2 e^{-iE_n t/\hbar}. \quad (2)$$

Here, the probability amplitude  $a_n$  can be obtained mathematically, and  $E_n$  defines the energy eigenvalue. The energy eigenvalue associated with the triangular well potential reads

$$E_n = (F^2 \hbar^2 / 2m)^{1/3} z_n, \quad (3)$$

where  $z_n$  are the zeros of the Airy function [32] and  $F = mg$ . In the case of large quantum numbers, it can be approximated as  $z_n = [(3\pi/2)(n - 1/4)]^{2/3}$ . Since the distribution  $|a_n|^2$  peaks around the average quantum number  $n_0$ , we expand the energy eigenvalue around the average quantum number  $n_0$ , such that  $\Delta n = n - n_0 \ll n_0$  [12]; therefore, we have

$$\exp\left(\frac{-iE_n t}{\hbar}\right) \cong \exp\left\{-i\left(E_{n_0} + \frac{2\pi(n - n_0)}{T_{\text{cl}}} + \frac{2\pi(n - n_0)^2}{T_{\text{rev}}} + \dots\right)\frac{t}{\hbar}\right\}. \quad (4)$$

The corresponding classical and quantum revival times for the RTM are  $T_{\text{cl}} = 2\sqrt{2mz_0/F}$  and  $T_{\text{rev}} = 16mz_0^2/\pi\hbar$ , respectively.

In order to study the time evolution, we calculate the absolute square of the autocorrelation function, defined as

$$g(t) = \sum_{n,m} |a_n|^2 |a_m|^2 e^{-iE_{nm} t/\hbar}, \quad (5)$$

where  $E_{nm} = E_n - E_m$ . The autocorrelation function for the material wave packet for a certain fixed position of the cantilever is shown in Fig. 1 b.

In the next section, we explain revival and fractional revivals in the time–frequency domain and plot a scalogram, which indicates them in the time–frequency plane and determines their order.

### 3. Time–Frequency Analysis

The continuous wavelet transform (CWT) for the autocorrelation function  $g(t)$  given in Eq. (5) is

$$T_{g(t)}(f, \tau) = \pi^{-1/4} \sqrt{f_0/f} \sum_{n,m} |a_n|^2 |a_m|^2 e^{-iE_{nm}\tau/\hbar} I_{nm}, \tag{6}$$

where  $I_{nm} = \int_{-\infty}^{+\infty} e^{-(iE_{nm}f_0\zeta)/f} e^{-2\pi i f_0 \zeta} e^{(-1/2)\zeta^2} d\zeta$ . Solving  $I_{nm}$  and using the Taylor series expansion of energy eigenvalues for  $n$  and  $m$ , as given in Eq. (4), for the CWT denoted as  $T_{g(t)}(f, \tau)$ , we obtain

$$T_{g(t)}(f, \tau) = v \sum_{n,m} |c_{n,m}|^2 e^{-ix_{nm}\tau} r_{n,m}. \tag{7}$$

where  $v = \pi^{-1/4} \sqrt{2\pi f_0/f}$ ,  $x_{nm} = 2\pi(n - m) [(1/T_{cl}) + (n + m - 2n_0)/T_{rev}]$ ,  $|c_{n,m}|^2 = |a_n|^2 |a_m|^2$ , and  $r_{n,m} = \exp [-(1/2) (2\pi f_0 + (f_0/f x_{nm}))^2]$ .

We perform a frequency domain analysis of the autocorrelation, in view of the fast Fourier transform (FFT), which is an efficient algorithm of generating the Fourier transform (FT).

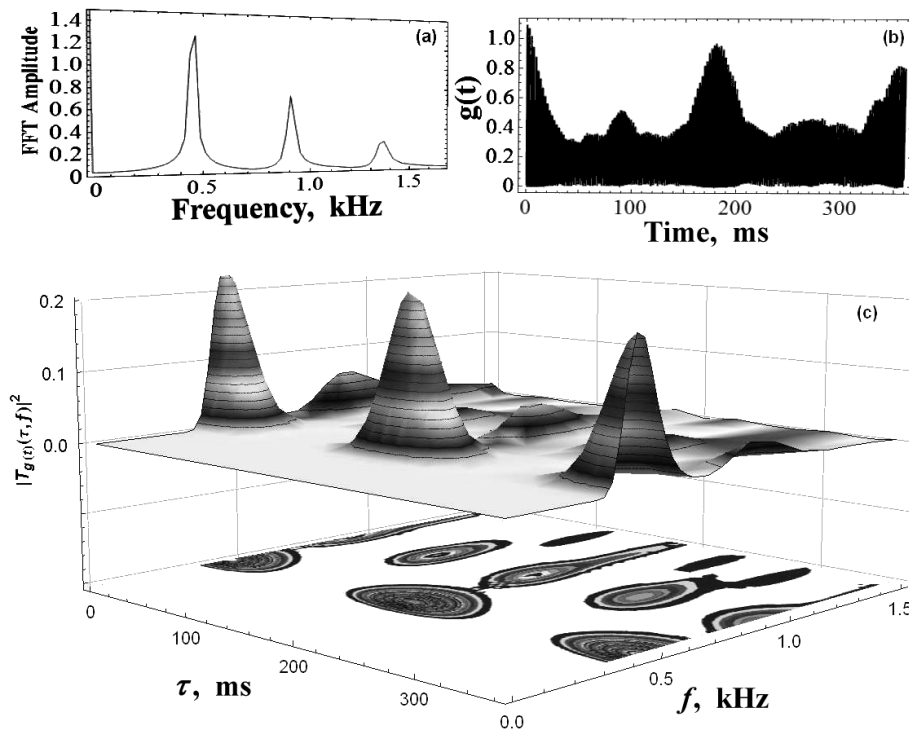


**Fig. 1.** The autocorrelation function of a material wave packet in a recurrence tracking microscope (a). We placed a Gaussian wave packet at  $z_0 = 5.65 \mu\text{m}$ , with  $\Delta z = 0.226 \mu\text{m}$  above the surface of the optical crystal at  $t = 0$  [31]. For the case of cesium (Cs) atom corresponding to the classical and revival times occurring at 2.14 and 348 ms, respectively, the FFT of the autocorrelation function determines all spectral components (b) and the time–frequency representation of the autocorrelation function (c) using the CWT, which explains the partial fractional revival across the corresponding frequency bands. Here,  $|T_{g(t)}(\tau, f)|^2$  is scaled by  $10^{-3}$ .

The main advantage of the FFT is its shorter execution time [34] due to the decrease in the number of calculations needed to analyze the waveform.

We plot the FFT of the autocorrelation function, which provides frequency components that exist in the autocorrelation function shown in Fig. 1 a. Each component of the autocorrelation function can be reconstructed across its frequency, which helps in understanding the role of frequency in quantum recurrence phenomena. Across each frequency band, as shown in Fig. 1 a, there exists a time harmonic, which can be reconstructed using CWT, as given in Eq. (7).

The CWT of the material wave packet  $T_{g(t)}(f, \tau)$  maps partial fractional revivals across their corresponding frequency bands, as shown in Fig. 1 c. This shows the role of favorable frequencies that contribute to fractional revivals of the wave packet. The sharp peaks and neighboring patches in the scalogram across different frequencies and times identify changes in amplitude of the autocorrelation function over the evolution time. Each sharp peak and corresponding patch appearing in the time–frequency distribution corresponds to a specific partial fractional revival of the wave packet.

The main advantage obtained from the continuous wavelet transform (CWT) is the reconstruction of the autocorrelation function for a specific frequency band and localization of fractional revivals in the time–frequency plane. It is important to note that the maximum value of the transformed function  $T_{g(t)}(f, \tau)$ , as given in Eq. (7), is at  $f = -x_{nm}/2\pi$ . Therefore, we obtain

$$f = (m - n) (1/T_{cl}) + [(m + n - 2n_0)/T_{rev}]. \quad (8)$$

Setting  $n = n_0$  and  $m = n_0 + y$ , we arrive at

$$f = (y/T_{cl}) [1 + yT_{cl}/T_{rev}]. \quad (9)$$

Considering the approximation as  $T_{cl}/T_{rev} \ll 1$ , we derive the central frequency of each frequency band, shown in Fig. 1 a and c, as follows:

$$f = (y/2)\sqrt{g/2z_0}, \quad (10)$$

where  $y$  is a positive integer,  $y = 1, 2, 3, 4 \dots$

The coherent addition of terms given in Eq. (6) would require that the terms corresponding to the time-dependent exponential be not dependent on  $n$  and  $m$ , i.e.,  $\tau E_{n,m} = \tau E_{n',m'}$ . Hence, the time  $\tau$  at which these terms add up coherently to give a peak structure is

$$\tau = (s/2y) T_{rev}, \quad (11)$$

where  $s$  is an integer such that  $s = 1, 2, 3 \dots$

From Eq. (10), we obtain the central frequency of the lowest band by setting  $y = 1$ . The time  $\tau = (s/2)T_{rev}$  corresponding to the lowest frequency band defines a specific set of partial fractional revivals, as shown in Fig. 2 a. Similarly, the set of partial fractional revivals occurring across the next frequency band ( $y = 2$ ) corresponds to  $\tau = (s/4)T_{rev}$ ; see Fig. 2 b. This process can be extended for higher frequency bands as well; see Fig. 2 c and d.

Across each frequency band, there is a specific set of partial fractional revivals. Hence, we conclude that Eqs. (10) and (11), respectively, provide the required resolution in frequency and measurement of time to reconstruct fractional revivals in the autocorrelation function.

A partial fractional revival seems to be more prominent, which helps to identify the exact location of a fractional revival. Hence, we note that the time–frequency analysis provides detailed information

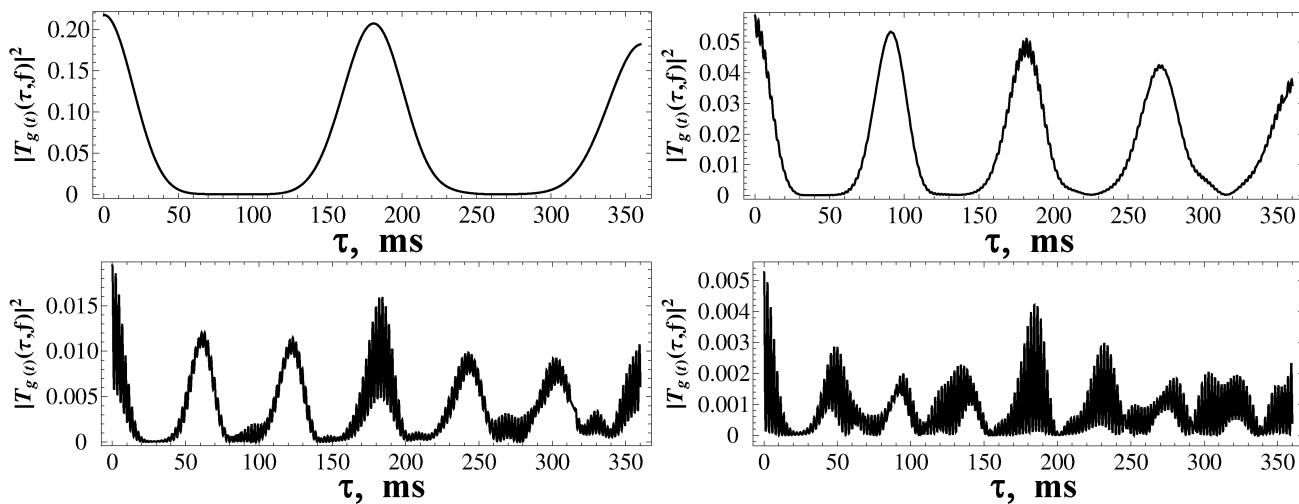


**Fig. 2.** The distribution  $|T_{g(t)}(\tau, f)|^2$  for  $f = 0.467$  KHz (a),  $0.935$  KHz (b),  $1.401$  KHz (c), and  $1.869$  KHz (d). Here,  $|T_{g(t)}(\tau, f)|^2$  is scaled by  $10^{-3}$ .

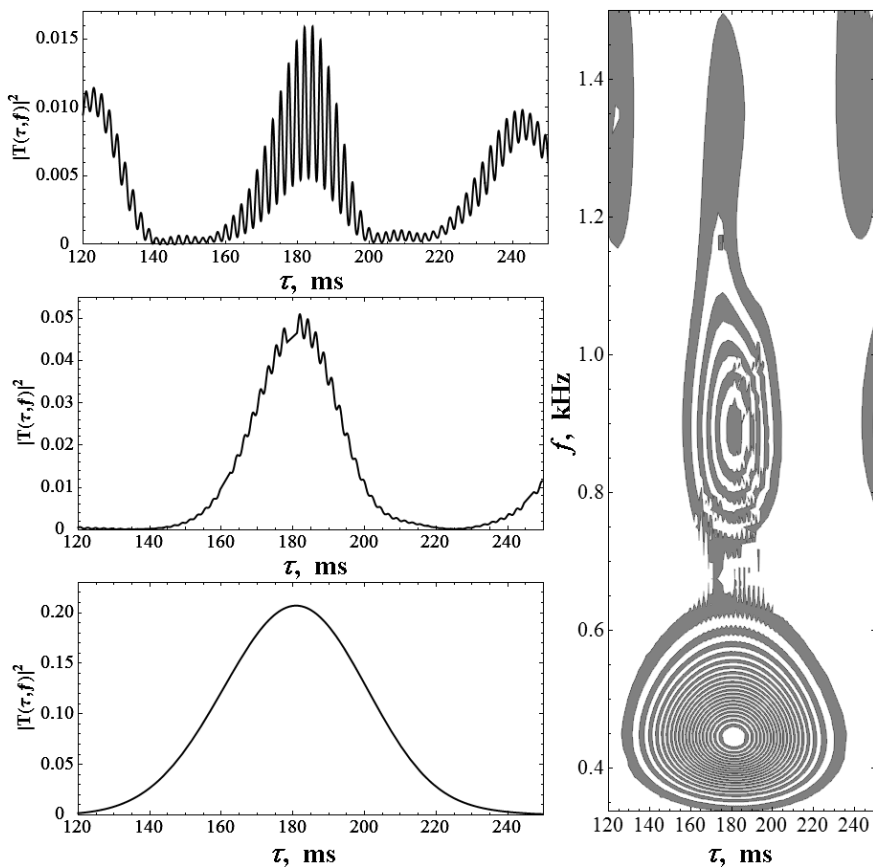


**Fig. 3.** The peaks corresponding to half fractional revival time as a function of time  $\tau$  (on the left). Here, the uncertainty around the revival time  $\Delta T$  is large for the lowest frequency band (c), whereas it decreases gradually for higher frequency bands (b and a). A section of the scalogram shows partial half-fractional revival in the frequency–time plane (on the right).

on the role of constructive and destructive interferences in quantum recurrences. The constructive and destructive interferences occur among time series harmonics, as shown in Fig. 2 a–d, resulting in periodic collapse and revival of the wave packet.

## 4. Resolution Enhancement in the RTM

A change in the initial height of the atom above the atomic mirror modifies the revival time. In the RTM, a variation of the revival time during an experiment measures the nanostructures on the surface under study. The revival of the wave packet  $T_{\text{rev}}$  corresponds to the initial height  $z_0$ , which varies as the cantilever moves up or down due to the nanostructures on the surface. The uncertainty  $\Delta T$  in measurement of the revival time is proportional to the uncertainty in the position of nanostructures  $\Delta z_0$ . We express  $\Delta z_0$  as

$$\Delta z_0 = \gamma \Delta T, \quad (12)$$

where  $\gamma = z_0/2T_{\text{rev}}$ . The reduction in uncertainty in the position of the cantilever corresponds to improved enhancement of the size of nanostructures on the sample surface. We write it as

$$a = a_1 + \Delta z_0, \quad (13)$$

where  $a_1$  is the size of the nanostructure and  $a$  is the experimentally observed size of the nanostructure with a certain uncertainty  $\Delta z_0$ .

The uncertainty in partial fractional revivals corresponding to higher frequency bands decreases drastically which, as a result, makes the time of revival measurements more certain, and this leads to a higher resolution in the measurements of the size of the nanostructure  $a$ . In Table 1, we show the results of calculations of  $\Delta T$  and  $\Delta z_0$  for partial half-fractional revival across various frequency bands, including higher frequency bands  $\Delta T$ ; as a consequence,  $\Delta z_0$  gradually decreases, which makes partial half fractional revival more localized around its occurrence time, as shown in Fig. 3.

We consider four different values of frequency, as shown in Table 1. As we switch the device to higher frequency, the quantity  $\Delta z_0$  decreases, and as a result the resolution of RTM becomes better.

**Table 1.** The Uncertainty  $\Delta T$  in Partial Half-Fractional Revival Time Calculated at  $(3/4)|T_{g(t)}(\tau, f)|^2$  and the Corresponding Uncertainty  $\Delta z_0$  in the Measurement of the Size of Nanostructures.

S. No.	Frequency, KHz	$\Delta T$ , ms	$\Delta z_0$ , nm
1	0.46	$\cong 5$	$\cong 4$
2	0.93	$\cong 2$	$\cong 1.96$
3	1.8	$\cong 1$	$\cong 0.9$
4	3.6	$\cong 0.7$	$\cong 0.68$

## 5. Conclusions

In this study, we showed that the application of the continuous wavelet transform (CWT) enables us to improve the resolution of a recurrence tracking microscope (RTM) to subnanometer scale. The approach developed provides a deeper insight into reading information on frequency bands, times of revivals, and corresponding times of fractional revivals more accurately. The presently suggested approach is implicable to enhance the resolution of the recurrence tracking microscopes based on the surface trap [35], a single magnetic mirror and two magnetic mirrors [36,37], and RTM based on the Bose–Einstein condensates [38–40].

## Acknowledgments

F. S. thanks the University of Electro-Communications and Jerash University for support and Shinichi Watanabe and Hui Jing for useful suggestions. N. A. acknowledges the CSC fellowship for financial support.

## References

1. P. Brault, J. Starck, and P. B. Beauvillian, *Phys. Rev. Lett.*, **76**, 459 (1996).
2. G. Binnig, C. F. Quate, and Ch. Gerber, *Phys. Rev. Lett.*, **56**, 930 (1986).
3. D. B. Williams and C. B. Carter, *Transmission Electron Microscope*, Springer (1996).
4. M. Auzinsh, D. Budker, D. F. Kimball, et al., *Phys. Rev. Lett.*, **93**, 173002 (2004).
5. G. Binnig and H. Rohrer, *Rev. Mod. Phys.*, **59**, 615 (1987).
6. E. Betzig, *Rev. Mod. Phys.* **87**, 1153 (2015).
7. S.W. Hell, *Rev. Mod. Phys.* **87**, 1169 (2015).
8. W.E. Moerner, *Rev. Mod. Phys.* **87**, 1183 (2015).
9. C. J. Chen, *Introduction to Scanning Tunnelling Microscopy*, Oxford University Press (2008).
10. V. Westphal and S. W. Hell, *Phys. Rev. Lett.*, **94**, 143903 (2005).
11. F. Saif, *Phys. Rev. A*, **73**, 033618 (2006).
12. R. W. Robinett, *Phys. Rep.*, **392**, 1 (2004).
13. F. Saif, *Phys. Rep.*, **419**, 207 (2005).
14. F. Saif, *Euro. Phys. J. D*, **39**, 87 (2006).
15. S. Iqbal, Q. ul Ann, and F. Saif, , **356**, 231 (2006). ??
16. F. Saif, *J. Opt. B: Quantum Semiclass. Opt.*, **7**, 116 (2005).
17. R. N. Bracewell, *The Fourier Transform and Its Applications*, McGraw-Hill Series in Electrical Engineering, Networks, and Systems (1986).
18. S. Mallat, *A Wavelet Tour of Signal Processing*, Academic Press (1999).
19. M. Chen, Q. Pang, J. Wang, and K. Cheng, *Int. J. Machine Tools Manufact.*, **48**, 905 (2008).
20. H. X. Wang, W. J. Zong, T. Sun, and Q. Liu, *Appl. Surf. Sci.*, **256**, 5061 (2010).
21. M. Grabka, S. Pustelny, P. Mergo, and W. Gawlik, *Opt. Express*, **20**, 13878 (2012).
22. P. Klapetek and I. Ohlidal, *Acta Phys. Slovaca*, **55**, 295 (2005).
23. P. Brault, J. L. Starck, and P. Beauvillain, "Characterization of nanostructures STM images with the wavelet and ridgelet transforms," in: *IAPR-ICISP03, International Conference on Image and Signal Processing (Agadir, Morocco, June 2003)*.
24. W. Cai, L. Wang, Z. Pan, et al., *J. Raman Spectrosc.*, **32**, 207 (2001).
25. S. Ghosh and J. Banerji, *J. Phys. B: At. Mol. Opt. Phys.*, **40**, 3545 (2007).
26. S.-A. Yahiaoui and M. Bentaiba, Los Alamos arXiv:1502.08007.
27. G. K. Brennen, P. Rohde, B. C. Sanders, and S. Singh, *Phys. Rev. A*, **92**, 032315 (2015).
28. F. Bulut and W. Polyzou, *Phys. Rev. D*, **87**, 116011 (2013).
29. M. V. Altaisky, *SIGMA*, **3**, 105 (2007).
30. M. V. Altaisky and N. E. Kaputkina, *Phys. Rev. D*, **88**, 025015 (2013).
31. J. Gea-Banacloche, *Am. J. Phys.*, **67**, 776 (1999).
32. O. Vallee and M. Soares, *Airy Functions and Applications to Physics*, Imperial College Press (2004).
33. W. H. Mather and R. F. Fox, *Phys. Rev. A*, **73**, 032109 (2006).

34. S. W. Smith, *The Scientist and Engineer's Guide to Digital Signal Processing*, California Technical Publishing, San Diego (2005).
35. F. Saif and M. Yameen, *J. Russ. Laser Res.*, **33**, 490 (2012).
36. F. Saif and M. Umar, *J. Russ. Laser Res.*, **34**, 154 (2013).
37. H. Ullah, M. Umar, M. Javed Akram, and F. Saif, *J. Russ. Laser Res.*, **35**, 401 (2014).
38. F. Saif and H. Ullah, "Recurrence tracking microscope based on Bose–Einstein condensates," in: *Proceedings of "Environment, Development, and Nanotechnology," Seventh International Scientific Conference, Al-Azhar University (ISCAZ 2010)*.
39. H. Ullah and F. Saif, *J. Russ. Laser Res.*, **31**, 408 (2010).
40. H. Ullah and F. Saif, *J. Russ. Laser Res.*, **37**, 1 (2017).